Supporting Information for

Spontaneous adsorption-oxidation of gaseous elemental mercury via a conjugated unit -$NH^{+\bullet}$-Cl*: creation and mechanisms

Zhao Ma[a], Runlong Hao*[,a,b], Tianxin Liu[a], Hongming Li[a], Jianping Yang[c], Zefeng Zeng[a], Bo Yuan[a,b], Meng Qi[a,b], Lidong Wang*[,b]

a. Hebei Key Lab of Power Plant Flue Gas Multi-Pollutants Control, Department of Environmental Science and Engineering, North China Electric Power University, Baoding, 071003, PR China

b. MOE Key Laboratory of Resources and Environmental Systems Optimization, College of Environmental Science and Engineering, North China Electric Power University, Beijing, 102206, PR China

c. School of Energy Science and Engineering, Central South University, Changsha, 410083, China

**Corresponding authors E-mail: hrl_ncepu@hotmail.com ; wld@ncepu.edu.cn*

Number of pages (including this page): 27

Number of texts: 6

Number of figures: 10

Number of tables: 4

1. All reagents and materials

The following reagents and materials are used in the synthesis process: polypropylene non-woven fabric (80g/m^2, Jinshengchang Guangdong China), multi-wall carbon nanotubes (Carboxylated MWCNTs, XFM21, XFNANO Nanjing China), aniline (AR, 99.5%, Macklin, 1.02g/mL), polyvinylidene fluoride (PVDF, FR905, Sanaifu Neimenggu China), N-methyl pyrrolidone (NMP, AR, 99%, Macklin), sodium dodecyl benzene sulfonate (SDBS, AR, 90%, Kermel Tianjin China), $(NH_4)_2S_2O_8$ (AR, 98%, Damao Tianjin China), HCl (AR, 36~38%, Damao Tianjin China), H_2SO_4 (AR, 95~98%, Damao Tianjin China), NaCl (AR, 99.5%, Kermel Tianjin China), ethanol absolute (AR, 99.7%, Huihang Tianjin China) , pyrrole (AR, 99%, Macklin, 0.97g/mL)and deionized water. The reagents in Hg^0 removal experiment and recovery: $KMnO_4$ (AR, 99.5%, Kermel Tianjin China), H_2SO_4 (AR, 95~98%, Damao Tianjin China), $SnCl_2{\cdot}2H_2O$ (AR, 98%, Kermel Tianjin China), NaCl (AR, 99.5%, Kermel), HCl (AR, 36~38%, Damao Tianjin China).

2. Synthesis procedure of 11PANI and 51PANI

The fabrication of 11PANI and 51PANI: 5 ml aniline and 0.16 ml HCl were added to 61 ml deionized water. Simultaneously, 12.52 g $(NH_4)_2S_2O_8$ was dissolved in 84 ml deionized water. Then, the latter was slowly poured into the former in ice bath. Next, the product was washed to neutral after 2 h. Finally, it was dried in vacuum drying oven at 60 ^oC for 12 h. The quality of $(NH_4)_2S_2O_8$ in the fabrication of 51PANI is fifth times that in the fabrication of 11PANI. 0.2 g 11PANI was dispersed into 100 ml deionized water. $11PANI^+$ (pH=0 or 1) was generated by immersion in H_2SO_4, Cl-11PANI was produced by immersion in 1 mol/L NaCl. $Cl\text{-}11PANI^+$ (pH=0 or 1) was produced by immersion in 1 mol/L NaCl at pH=0 or 1. The immersion time is 60 min and then the samples were dried in vacuum drying oven at 60 ^oC for 12 h.

3. Fabrication of the Composite Film

Figure S2 shows the fabrication process of composite film, including vacuum filtration, immersion and phase inversion methods. All reagents are listed in Text S1. Firstly, polyvinylidene fluoride (PVDF) and aniline were dissolved in N-methyl-pyrrolidone (NMP) solution under the condition of stirring and heating at 60 ^{o}C. And MWCNTs were dispersed in deionized water via ultrasonic treatment (ATPIO-1200D ATPIO Co., Nanjing China) at 720W for 5 min. Then, the dispersion was attached onto the surface of polypropylene non-woven fabric (NWF) by vacuum filtration method to form a thin framework layer (a filter paper was placed under NWF for retaining MWCNTs on NWF). Next, the film was immersed in the above NMP solution for 2 h. Then the film, containing about 2ml NMP solution, was picked up, and then immediately immersed into a 20ml mixture solution containing 1 mol/L H_2SO_4, 3mg/ml sodium dodecyl benzene sulfonate (SDBS) and 0.45g $(NH_4)_2S_2O_8$ (the molar ratio of $(NH_4)_2S_2O_8$ and aniline was 1:1), where the phase inversion of PVDF and the polymerization induced by $(NH_4)_2S_2O_8$ would take place simultaneously. Finally, the film was washed by deionized water and absolute ethanol, and dried in a vacuum drying oven (DZF-6020 Keelrein Co., Shanghai China) for 12 h at 60 ^{o}C. Accordingly, the film was marked as 11PANI@MWCNTs. The molar ratio of $(NH_4)_2S_2O_8$ and aniline will be 5:1 when 51PANI@MWCNTs is synthesized. Before the Hg^0 removal experiment, the film needed to be immersed in Cl-containing solution at pH=1 for 60 min and then dried, marked as Cl-$PANI^+$@MWCNTs. If without specific instructions, Cl-11$PANI^+$@MWCNTs is obtained via immersing 11PANI@MWCNTs into 1 mol/L NaCl at pH=1 for 60 min and drying.

4. Regeneration and recycling

To assess the reusability of the composite film, we carried out recycling tests after the film regeneration, at the gas flow of 1 L/min, about 200,000 h^{-1}. The regeneration of the composite membrane was realized through following procedure: the spent film was first immersed in a mixed solution of 1 mol/L NaCl at pH=1 (adjusted by H_2SO_4) for 60 min and then was dried. In the 5 cycles, the same solution is reused. In order to determine the proportion of mercury in the solution after 5 cycles, we used AFS to determine the mercury concentration in the leaching solution. As we all know, mercury balance is crucial for this test, thus we first determined the amount of Hg^0 discharged from mercury osmotic tube under a certain interval of 60 min, with 10% (v/v) H_2SO_4-4% (w/w) $KMnO_4$ solution as the capturing solution. The result indicated that the average output mass of Hg^0 (5 parallel tests) was approximately 15.1 μg in 60 min. Afterwards, in every cycle, Hg^0 removal experiment was terminated when the outlet concentration is more than 5% of the inlet concentration and then leached in acidic NaCl solution for 60 min. The mercury concentration in the leaching solution was finally determined by AFS, from which the quantity of the recovered mercury was obtained.

5. Characterization and DFT Calculation Methods

The morphology of the composite film was observed by a field emission scanning electron microcopy (FESEM, Hitachi-s4800). Energy-dispersive spectroscopy (EDS) was recorded by a Bruker quantax400 attached to the Hitachi-s4800 FESEM instrument to determine the elemental distribution of the composite film. The specific surface area (S_{BET}) and pore volume (V_P) were calculated by applying Brunauer-Emmett-Teller (BET) and Barrett-Joyner-Halina (BJH) models to the N_2 adsorption-desorption isotherms. The ultraviolet-visible spectra (UV-Vis) of polyaniline in different states were recorded by a UV-Vis spectrometer (TU-1901, Persee Co., Beijing China). And the surface functional groups were identified by a Fourier transform infrared spectrometer (FTIR, Nicolet iZ10). To determine the difference of every elemental valence in the composite film before and after the experiment, the binding energies of C 1s, O 1s, N 1s, F 1s, Cl 2p and Hg 4f were analyzed with X-ray photoelectron spectroscopy (XPS) (ESCALAB250 spectrometer with Al Kα source (1486.6 eV)). Density functional theory (DFT) is widely used to calculate the ground-state electronic structure of atoms, molecules, and solid-state materials, so the DFT calculations were also performed to clarify the reaction mechanism by using Gaussian 09 software.[1] The def2SVP was used to optimize the structures of molecules and calculate the single point energies based on the M062X in open shell with DFT-D3(BJ) and ultrafine integral grid.[2,3] And all data about model construction and optimization are shown in Table S4.

6. UV-Vis analyses procedure

In the UV-Vis experiment, the pure 11PANI and 51PANI were used, due to the required soluble samples, but MWCNTs is insoluble in NMP. The UV-Vis analysis procedure is as follows: NMP was used as reference solution. The above samples, synthesized in Text S2, were dissolved into NMP and all the concentrations were 0.05 g/L. The ultraviolet-visible spectrophotometer (TU-1901, Persee, Beijing China) was used to scan the absorption spectra of the samples in the range of 190-900 nm.

Figures

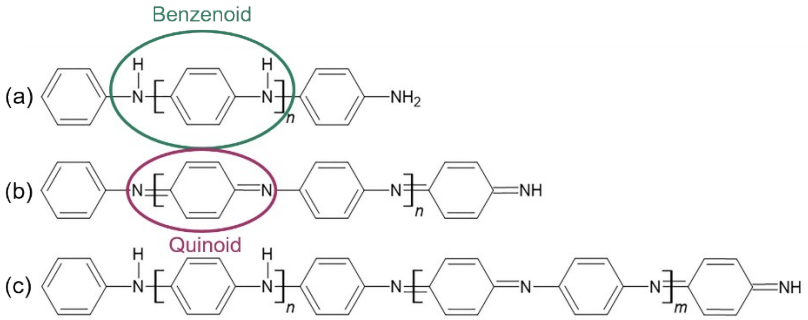

Figure S1. The molecular structures of (a) leucoemeraldine, (b) pernigraniline bases, (c) emeraldine.

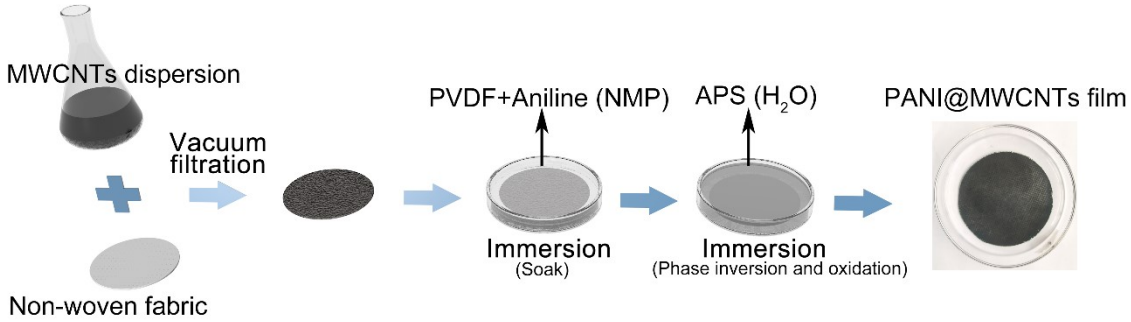

Figure S2. Fabrication procedures of the PANI@MWCNTs film.

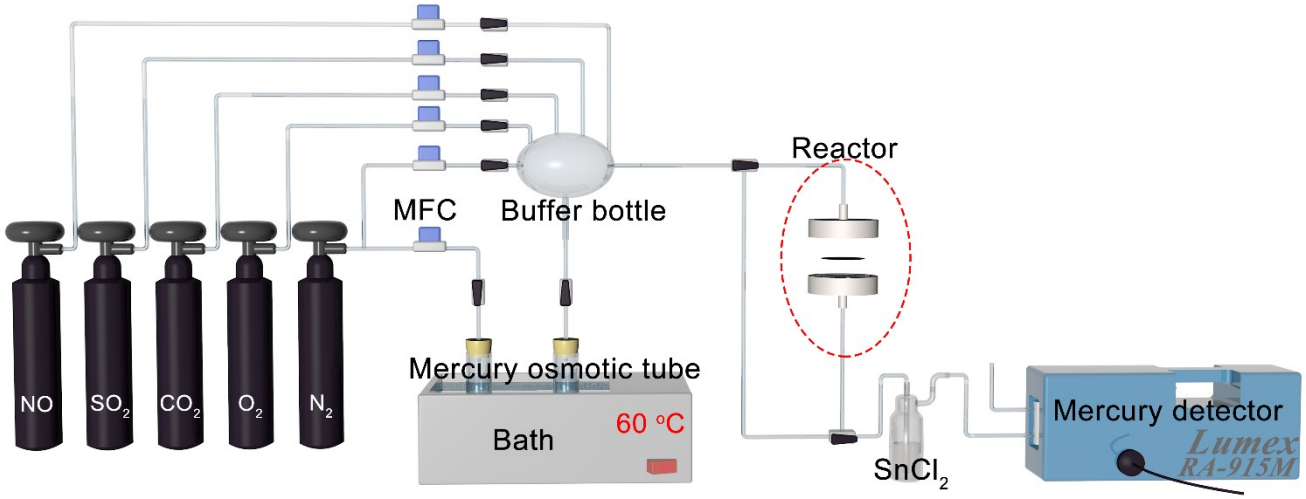

Figure S3. Scheme of Hg^0 removal experiment.

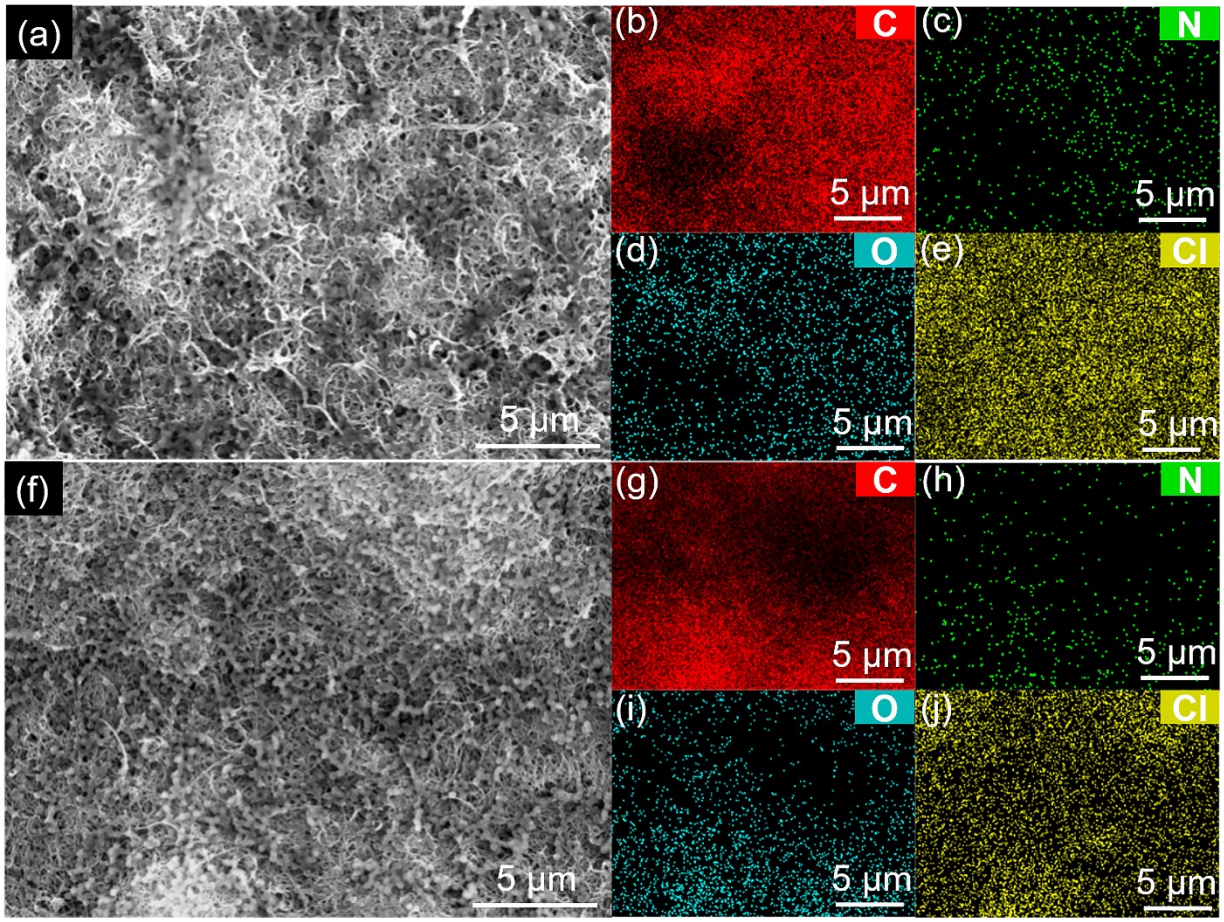

Figure S4. EDS and element mapping of the (a)-(e) Cl-11PANI^{+}@MWCNTs and (f)-(j) Cl-51PANI^{+}@MWCNTs film.

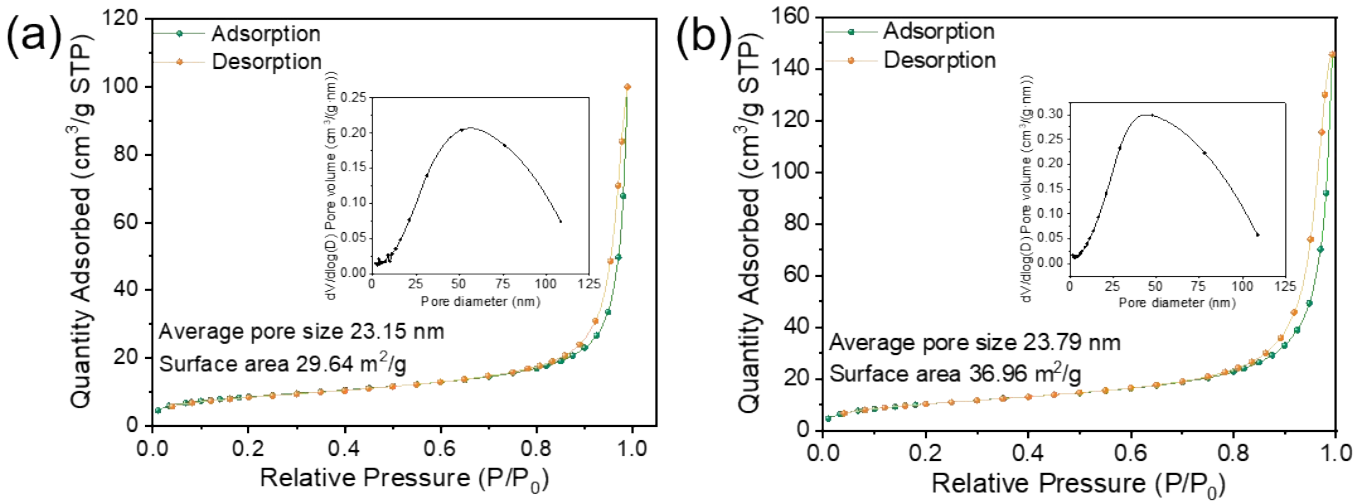

Figure S5. the BET results and BJH desorption pore diameter distribution of (a) Cl-11PANI^{+}@MWCNTs and (b) Cl-51PANI^{+}@MWCNTs

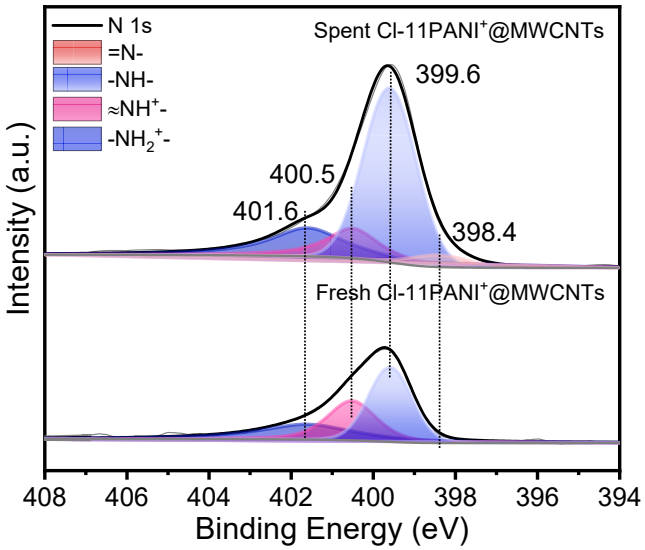

121 .

122 **Figure S6.** High-resolution N 1s XPS spectra of the fresh and spent Cl-11PANI^{+}@MWCNTs

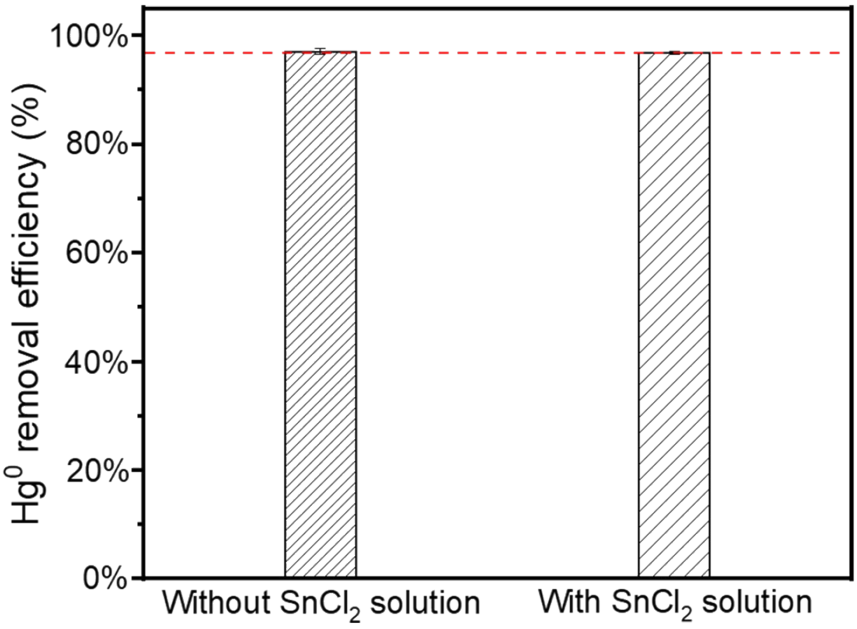

Figure S7. The Hg^0 removal efficiencies with and without $SnCl_2$ solution (Cl-11PANI$^+$@MWCNTs and the space velocity is 200,000 h^{-1})

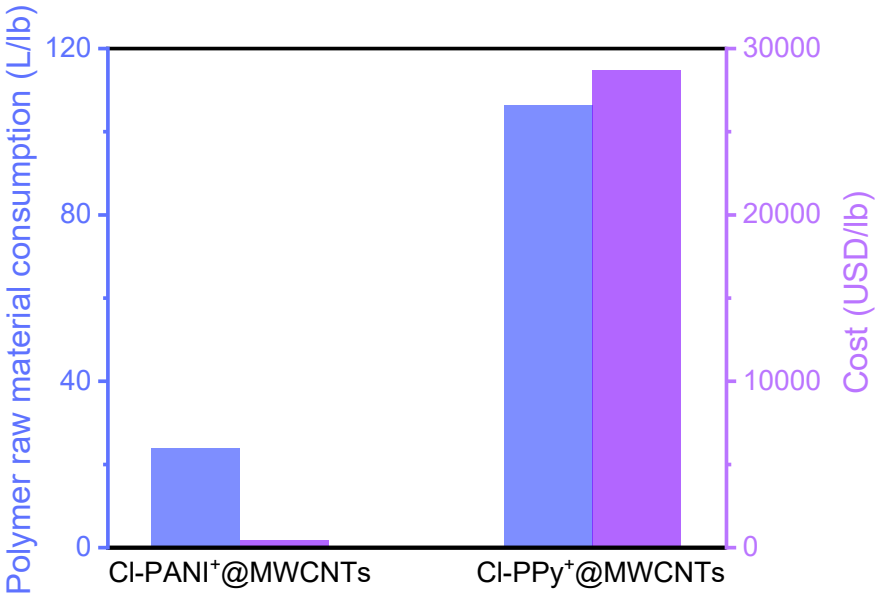

Figure S8. The polymer raw material consumption and cost.

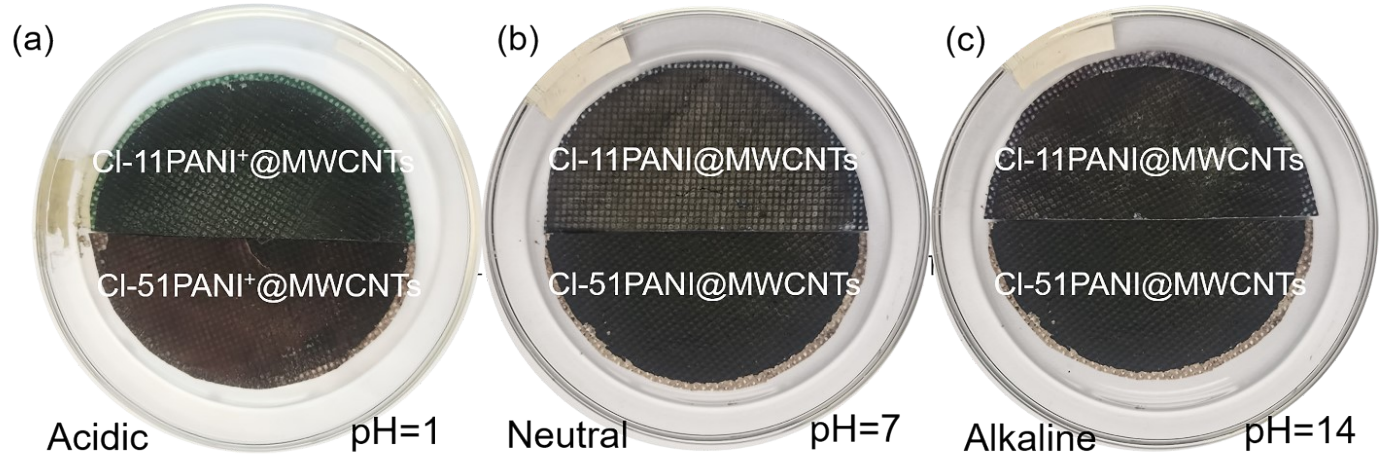

Figure S9. The macroscopic images of Cl-11PANI$^+$@MWCNTs and Cl-51PANI$^+$@MWCNTs at different pH.

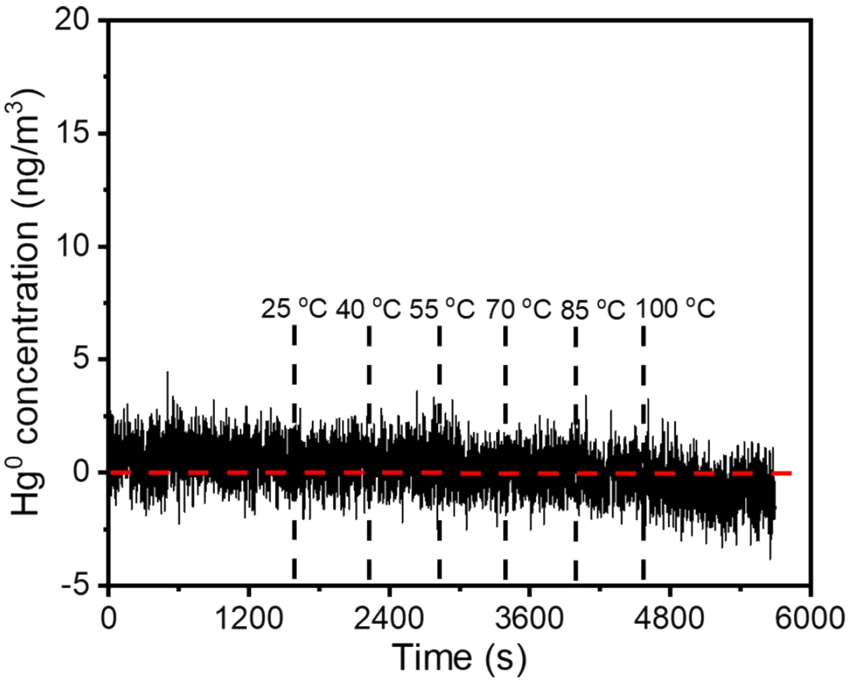

Figure S10. Stability of adsorbed mercury on the composite membrane under different temperatures. The Cl-11PANI^{+}@MWCNTs film was pretreated via gaseous Hg^0 for 1 h, concentration unit is ng/m^3, space velocity is 200,000 h^{-1}.

Table S1. Abbreviations in the work.

Abbreviated title	Title
MWCNTs	Multiwall carbon nanotubes
PANI	Polyaniline, and aniline is its monomer
11PANI	PANI synthesized in the molar ratio of $(NH_4)_2S_2O_8$ to aniline is 1:1
51PANI	PANI synthesized in the molar ratio of $(NH_4)_2S_2O_8$ to aniline is 5:1
$11PANI^+$	Protonated 11PANI
$51PANI^+$	Protonated 51PANI
Cl-$11PANI^+$	Cl-doped protonated 11PANI
Cl-$51PANI^+$	Cl-doped protonated 51PANI
11PANI@MWCNTs	11PANI coated MWCNTs
51PANI@MWCNTs	51PANI coated MWCNTs
$11PANI^+$@MWCNTs	Protonated 11PANI@MWCNTs
$51PANI^+$@MWCNTs	Protonated 51PANI@MWCNTs
Cl-$11PANI^+$@MWCNTs	Cl-doped protonated 11PANI@MWCNTs
Cl-$51PANI^+$@MWCNTs	Cl-doped protonated 51PANI@MWCNTs
Cl-PPy@MWCNTs or Cl-PPy^+@MWCNTs	Cl-doped protonated polypyrrole coated multiwall carbon nanotubes

Table S2 The element ratio of different films.

Materials	C (Wt%)	O (Wt%)	N (Wt%)	Cl (Wt%)	Others (Wt%)
Cl-11PANI^{+}@MWCNTs	86.0	3.0	2.1	5.4	3.5
Cl-51PANI^{+}@MWCNTs	92.0	3.2	1.2	1.9	1.7

141 **Table S3** Paper summary about the method for gaseous Hg^0 removal recently.

No.	Materials	Theory	Experimental conditions	Efficiency	adsorption capacity	Breakthrough point (output/input)	Cycle	Publication	Reference
1	MnO_x/Graphene	Adsorption and oxidation	- 0.5 L/min - 100-300 °C	>90%	2.7mg/g	10h	good	EST/2015,49,6823-6830	(4)
2	$LaMnO_3$	Catalytic oxidation and adsorption	500 μg/m^3 0.5 L/min 478000 h^{-1} 150 °C	>85%	6.22mg/g	50%	≥5	ACB/186(2016)30-40	(5)
3	CoMoS/γ-Al_2O_3	Adsorption	30 μg/m^3 1.5 L/min 45000 cm^3/(g·h) 25-450 °C	100% (50 °C)	18.95 mg/g	100% Elovich model	-	EST/2016,50,1056-1064	(6)
4	IrO_2/$Ce_{0.6}Zr_{0.4}O_2$	Catalytic oxidation and adsorption	370-1500 ng/m^3 0.5L/min 760000 h^{-1} 350 °C	>99%	-	-	good	EST/2016,50,2564-2572	(7)
5	Sawdust-Fe^{3+}	Adsorption and oxidation	85 μg/m^3 1.2 L/min - 120-250 °C	>90%	1.28 mg/g	100% Model simulation	-	EST/2016,50,12040-12047	(8)
6	nano-ZnS	Adsorption	65 μg/m^3 1 L/min - 140-260 °C	>90%	497.84 μg/g	50%	-	EST/2016,50,9551-9557	(9)

7	$[MoS_4]^{2-}$ /CoFe-LDH	Physical adsorption	350 μg/m^3 0.5 L/min - 50-150 °C	>95%	16.39 mg/g	3000-3250 min	-	EST/2017,51,10109-10116	(10)
8	Manganese Ore	Adsorption	65 μg/m^3 1 L/min - 100-250 °C	>90%	53.57 mg/g	100% Model fit	≥5	EST/2017,51,10109-10116	(11)
9	Ag-SBA-15 nanocomposite	Adsorption	125 μg/m^3 1 L/min 260000 h^{-1} 150 °C	>90%	13.2 mg/g;	1%	≥5	EST/2017,51,11909-11917	(12)
10	Nano-Sulfide	Adsorption and oxidation	75 μg/m^3 1 L/min 300000 cm^3/(g·h) 60-240 °C	>99%	-	-	-	EST/2018,52,12926-12933	(13)
11	Cl-biochar	Adsorption	20 μg/m^3 2 L/min - 150 °C	>80%	583.0 μg/g	90 min	-	CEJ/331(2018)536-544	(14)
12	3D MnO_2/CS	Adsorption	- 0.5 L/min - 100-300 °C	>99%	-	-	-	JHM/342(2018)69-76	(15)
13	O_2 and NO Co-Doped Porous Carbon	Adsorption	50 μg/m^3 1 L/min 76000 h^{-1} 120 °C	>90%	12.3 mg/g	100% Model simulation	-	EST/2019,53,1725-1731	(16)

14	HNO_3-treated activated carbon fiber cloth (ACFC)	Adsorption	260-300 μg/m^3 0.5 L/min - -	>90%	-	-	≥9	EST/2020,54,1857-1866	(17)
15	Ti-sulfurated γ-Fe_2O_3	Adsorption and oxidation	4300 μg/m^3 300 mL/min 1200000 h^{-1} 40-100 °C	-	48.6 mg/g	10 h	≥5	JHM/381(2020)120967	(18)
16	AMn_2O_4 (A=Cu, Ni and Zn)	Adsorption	50 μg/m^3 1 L/min 50000 h^{-1} 200 °C	>95%	25.6 mg/g	50%	good	JHM/338(2020)121738	(19)
17	V_2O_5-MoO_3/TiO_2	Adsorption and oxidation	110 μg/m^3 0.5 L/min 3000000 cm^3/(g·h) 80 °C	79%	0.433 mg/g	40%	≥5	EST/2021,55,7072-7081	(20)
18	nano-ZnS	Adsorption	190 μg/m^3 - 150000 h^{-1} 60-220 °C	-	0.27 mg/g	50%	-	EST/2021,55,6965-6974	(21)
19	Single-Site Manganese	Adsorption	1200 μg/m^3 0.5 L/min - 25-550 °C	>97% (<200 °C)	>13 mg/g	-	-	EST/2021,55,20,14126-14135	(22)
20	Spherical-shaped CuS/C_3N_4 nanosheet	Adsorption	95 μg/m^3 1.2 L/min - 40-120 °C	100%	-	-	-	JHM/415(2021) 125692	(23)

142

Table S4. The DFT calculation data

Structure	State	Charge	E_t(a.u.)	ΔE_t(a.u.)	ΔG(kJ/mol)
Cl^-	singlet	-1	-460.082984	-	-
H^+	singlet	+1	-0.010000	-	-
Hg	singlet	0	-153.420286	-	-
Hg-Hg	singlet	0	-306.836414	-	-
11PANI	singlet	0	-1429.913820	-	-
$11PANI^+$	singlet	+2	-1430.605571	-0.671751	-1763.48
$11PANI^+$	triplet	+2	-1430.637001	-0.031430	-82.51
$Cl\text{-}11PANI^+$	singlet	0	-2351.220459	-0.448920	-1178.50
$Cl\text{-}11PANI^+$	triplet	0	-2351.199161	-0.396192	-1040.08
$Hg\text{-}Cl\text{-}11PANI^+$	**singlet**	**0**	**-2658.108806**	**-0.051933** **-0.073231**	**-136.33** **-192.25**
51PANI	singlet	0	-1428.680652	-	-
$51PANI^+$	singlet	+2	-1429.388896	-0.688244	-1806.78
$51PANI^+$	triplet	+2	-1429.371210	0.017686	46.43
$Cl\text{-}51PANI^+$	singlet	0	-2349.986134	-0.431270	-1132.17
$Cl\text{-}51PANI^+$	triplet	0	-2349.957207	-0.420029	-1102.66
$Hg\text{-}Cl\text{-}51PANI^+$	**singlet**	**0**	**-2656.824779**	**-0.002231** **-0.031158**	**-5.86** **-81.80**

References

(1) Frish, M. J.; Trucks, G. W.; , et al. Gaussian 09, Revision E.01; Gaussian, Inc.: Wallingford, CT, 2013.

(2) Yan, Z.; Truhlar, D. G. The M06 suite of density functionals for main group thermochemistry, thermochemical kinetics, noncovalent interactions, excited states, and transition elements: two new functionals and systematic testing of four M06-class functionals and 12 other functionals. *Theor. Chem. Acc.* **2008**, *119*(1-3), 525.

(3) Grimme, S.; Antony, J.; Ehrlich, S.; Krieg, H. A consistent and accurateab initio parametrization of density functional dispersion correction (DFT-D) for the 94 elements H-Pu. *The Journal of Chemical Physics*. **2010**, *132*(15), 154104.

(4) Xu, H. M.; Qu, Z.; Huang, W. J.; Quan, F. Q.; Yan, N. Q. MnOx/Graphene for the catalytic oxidation and adsorption of elemental mercury. *Environ. Sci. Technol.* **2015**, *49*, 6823-6830.

(5) Xu, H. M.; Qu, Z.; Zong, C. X.; Quan, F. Q.; Mei, J.; Yan, N. Q. Catalytic oxidation and adsorption of Hg^0 over low-temperature NH_3-SCR $LaMnO_3$ perovskite oxide from flue gas. *Appl. Catal. B*. **2016**, *186*, 30-40.

(6) Zhao, H. T.; Yang, G.; Gao, X.; Pang, C. H.; Kingman, S. W.; Wu, T. Hg^0 capture over CoMoS/γ-Al_2O_3 with MoS_2 nanosheets at low temperatures. *Environ. Sci. Technol.* **2016**, *50*, 1056-1064.

(7) Chen, W. M.; Pei, Y.; Huang, W. J.; Qu, Z.; Hu, X. F.; Yan, N. Q. Novel effective catalyst for elemental mercury removal from coal-fired flue gas and the mechanism investigation. *Environ. Sci. Technol.* **2016**, *50*, 2564-2572.

(8) Yang, J. P.; Zhao, Y. C.; Ma, S.; Zhu, B. B.; Zhang, J. Y.; Zheng, C. G. Mercury removal by magnetic biochar derived from simultaneous activation and magnetization of sawdust. *Environ. Sci. Technol.* **2016**, *50*, 12040-12047.

(9) Li, H. L.; Zhu, L.; Wang, J.; Li, L. Q.; Shih, K. Development of nano-sulfide sorbent for efficient removal of elemental mercury from coal combustion fuel gas. *Environ. Sci. Technol.* **2016**, *50*, 9551-9557.

(10) Xu, H. M.; Yuan, Y.; Xie, J. K.; Qu, Z.; Shangguan, W. F.; Yan, N. Q. $[MoS_4]^{2-}$ cluster bridges in Co−Fe layered double hydroxides for mercury uptake from S−Hg mixed flue gas. *Environ. Sci. Technol.* **2017**, *51*, 10109-10116.

(11) Yang, Y. J.; Miao, S.; Liu, J.; Wang, Z.; Yu, Y. N. Cost-effective manganese ore sorbent for elemental mercury removal from flue gas. *Environ. Sci. Technol.* **2017**, *51*, 10109-10116.

(12) Cao, T. T.; Li, Z.; Xiong, Y.; Yang, Y.; Xu, S. M.; Bisson, T.; Gupta, R.; Xu, Z. H. Silica-silver nanocomposites as regenerable sorbents for Hg^0 removal from flue gases. *Environ. Sci. Technol.* **2017**, *51*, 11909-11917.

(13) Zhao, J. X.; Li, H. L.; Yang, Z. Q.; Zhu, L.; Zhang, M. G.; Feng, Y.; Qu, W. Q.; Yang, J. P.; Shih, K. Dual roles of nano-sulfide in efficient removal of elemental mercury from coal combustion flue gas within a wide temperature range. *Environ. Sci. Technol.* **2018**, *52*, 12926-12933.

(14) Wang, T.; Liu, J.; Zhang, Y. S.; Zhang, H. C.; Chen, W. Y.; Norris, P.; Pan, W. P. Use of a non-thermal plasma technique to increase the number of chlorine active sites on biochar for improved mercury removal. *Chem. Eng. J.* **2018**, *331*, 536-544.

(15) Xu, H. M.; Jia, J. P.; Guo, Y. F.; Qu, Z.; Liao, Y.; Xie, J. K.; Shangguan, W. F.; Yan, N. Q. Design of 3D MnO_2/Carbon sphere composite for the catalytic oxidation and adsorption of elemental mercury. *J. Hazard. Mater.* **2018**, *342*, 69-76.

(16) Shen, F. H.; Liu, J.; Wu, D. W.; Dong, Y. C.; Zhang, Z. Development of O_2 and NO co-doped porous carbon as a high-capacity mercury sorbent. *Environ. Sci. Technol.* **2019**, *53*, 1725-1731.

(17) Chen, B. C.; Tsai, C. Y.; Pan, S. Y.; Chen, Y. T.; His, H. C. Sustainable recovery of gaseous mercury by adsorption and electrothermal desorption using activated carbon fiber cloth. *Environ. Sci. Technol.* **2020**, *54*, 1857-1866.

(18) Mei, J.; Wang, C.; Kong, L. N.; Sun, P. X.; Hu, Q. X.; Zhao, H.; Guo, Y. F.; Yang, S. J. Remarkable

improvement of Ti incorporation on Hg^0 capture from smelting flue gas by sulfurated γ-Fe_2O_3: Performance and mechanism. *J. Hazard. Mater.* **2020**, *318*, 120967.

(19) Wang, Z.; Liu, J.; Yang, Y. J.; Yu, Y. N.; Yan, X. C.; Zhang, Z. AMn_2O_4 (A=Cu, Ni and Zn) sorbents coupling high adsorption and regeneration performance for elemental mercury removal from syngas. *J. Hazard. Mater.* **2020**, *388*, 121738.

(20) Wang, C.; Hong, Q. Q.; Ma, C.; Mei, J.; Yang, S. J. Novel promotion of sulfuration for Hg^0 conversion over V_2O_5–MoO_3/TiO_2 with HCl at low temperatures: Hg^0 adsorption, Hg^0 oxidation, and Hg^{2+} adsorption. *Environ. Sci. Technol.* **2021**, *55*, 7072-7081.

(21) Yang, Y.; Huang, R.; Xu, W. Q.; Zhang, J. X.; Li, C. Q.; Song, J. F.; Zhu, T. Y. Different crystal forms of ZnS nanomaterials for the adsorption of elemental mercury. *Environ. Sci. Technol.* **2021**, *55*, 6965-6974.

(22) Li, J. X.; Xu, H. M.; Huang, Q. Y.; Qiu, Y. X.; Yan, N. Q.; Qu, Z. Strengthen the affinity of element mercury on the carbon-based material by adjusting the coordination environment of single-site manganese. *Environ. Sci. Technol.* **2021**, *55*, 14126-14135.

(23) Wang, F. J.; Wang, R.; Jia, T.; Wu, J.; Xu, C. F.; Sun, Y.; Wang, X.; Wu, W. Y.; Qi, Y. F. Spherical-shaped CuS modified carbon nitride nanosheet for efficient capture of elemental mercury from flue gas at low temperature. *J. Hazard. Mater.* **2021**, *415*, 125692.